






Article

Self-Assembly of Copper Oxide Interfaced MnO₂ for Oxygen Evolution Reaction

Chinna Bathula¹, Abhishek Meena², Sankar Sekar^{3,4} , Aditya Narayan Singh⁵ , Ritesh Soni⁶ , Adel El-Marghany⁷, Ramasubba Reddy Palem⁸  and Hyun-Seok Kim^{1,*} 

¹ Division of Electronics and Electrical Engineering, Dongguk University–Seoul, Seoul 04620, Republic of Korea; cdbathula@dongguk.edu

² Division of Physics and Semiconductor Science, Dongguk University–Seoul, Seoul 04620, Republic of Korea; pakar.abhishek@gmail.com

³ Department of Semiconductor Science, Dongguk University–Seoul, Seoul 04620, Republic of Korea; sanssekar@gmail.com

⁴ Quantum-Functional Semiconductor Research Center, Dongguk University–Seoul, Seoul 04620, Republic of Korea

⁵ Department of Energy and Materials Engineering, Dongguk University–Seoul, Seoul 04620, Republic of Korea; aditya@dongguk.edu

⁶ Department of Chemical Engineering, Department of Energy Engineering, Ulsan National Institute of Science and Technology (UNIST), 50 UNIST-gil, Ulsan 44919, Republic of Korea; riteshsoni@unist.ac.kr

⁷ Department of Chemistry, College of Science, King Saud University, P.O. Box 2455, Riyadh 11451, Saudi Arabia; amarghany@ksu.edu.sa

⁸ Department of Medical Biotechnology, Dongguk University, 32 Dongguk-ro, Ilsandong-gu, Goyang 10326, Republic of Korea

* Correspondence: hyunseokk@dongguk.edu

Abstract: Designing efficient electrocatalytic systems through facile synthesis remains a formidable task. To address this issue, this paper presents the design of a combination material comprising two transition metal oxides (copper oxide and manganese oxide (CuO/MnO₂)), synthesized using a conventional microwave technique to efficiently engage as an active oxygen evolution reaction (OER) catalyst. The structural and morphological properties of the composite were confirmed by the aid of X-ray diffraction (XRD) studies, field emission scanning electron microscopy (FESEM), X-ray photoelectron spectroscopy (XPS), and energy-dispersive spectrometry (EDS). FESEM clearly indicated well-aligned interlacing of CuO with MnO₂. The OER performance was carried out in 1 M KOH. The assembled CuO/MnO₂ delivered a benchmark current density ($j = 10 \text{ mA cm}^{-2}$) at a minimal overpotential ($\eta = 294 \text{ mV}$), while pristine CuO required a high η (316 mV). Additionally, the CuO/MnO₂ electrocatalyst exhibited stability for more than 15 h. These enhanced electrochemical performances were attributed to the large volume and expanded diameter of the pores, which offer ample surface area for catalytic reactions to boost OER. Furthermore, the rate kinetics of the OER are favored in composite due to low Tafel slope (77 mV/dec) compared to CuO (80 mV/dec).

Keywords: CuO/MnO₂; oxygen evolution reaction; electrocatalyst; stability



Citation: Bathula, C.; Meena, A.; Sekar, S.; Singh, A.N.; Soni, R.; El-Marghany, A.; Palem, R.R.; Kim, H.-S. Self-Assembly of Copper Oxide Interfaced MnO₂ for Oxygen Evolution Reaction. *Nanomaterials* **2023**, *13*, 2329. <https://doi.org/10.3390/nano13162329>

Academic Editors: Wei Zhang and Weitao Zheng

Received: 31 July 2023

Revised: 8 August 2023

Accepted: 11 August 2023

Published: 13 August 2023



Copyright: © 2023 by the authors. Licensee MDPI, Basel, Switzerland. This article is an open access article distributed under the terms and conditions of the Creative Commons Attribution (CC BY) license (<https://creativecommons.org/licenses/by/4.0/>).

1. Introduction

In the pursuit of achieving a carbon-neutral society and to alleviate the harmful effects of conventional fossil fuels, there is a pressing need to develop sustainable, eco-responsive, and green energy sources. To cater to fossil fuel resource depletion and its associated environmental impacts, in addition to the dynamic geopolitical instabilities of fossil fuel production, energy researchers have explored numerous sustainable energy sources such as wind, biomass, tidal, and solar energy. Among these available energy resources, solar radiation is one of the most abundant natural energy sources, capable of meeting the entire global energy demand, but it suffers from intermittent availability due to geographical

variations [1,2]. Furthermore, the sun shines only for a part of the day and its power density varies as the function of geographical altitude imposes another complexity to its wider applicability. Additionally, with the recent progress in photovoltaic devices, the power convergence efficiency hardly reached ~26% [3], further jeopardizing the adequacy of solar power [4]. Among several available renewable energy sources, splitting water ($2\text{H}_2\text{O} = 2\text{H}_2 + \text{O}_2$) to generate useful hydrogen as a fuel and oxygen as a by-product has drawn substantial attraction, as the generated hydrogen can be stored and can be transported at the required site. However, water electrolysis is an energy-intensive process, and its efficiency is limited by the sluggish kinetics of the oxygen evolution reaction (OER) at the anode. The OER proceeds via a four-electron process and involves the formation of two oxygen–oxygen bonds, and thus determines the overall rate kinetics of the water electrolysis [5]. Theoretically, OER requires a thermodynamic potential of 1.23 V (25 °C/1 atm); however, the commercial catalysts require much higher overpotentials (η). To date, Ir- and Ru-based electrocatalysts have been the best-performing OER electrocatalysts in aqueous media. However, their scarcity and prohibitive cost pose a major obstacle towards widespread use of electrolysis technologies. Therefore, significant efforts have been made in recent years to develop efficient and cost-effective OER catalysts that can enhance the performance of water electrolysis and enable the large-scale production of green hydrogen [6–8]. Of note, several 3D transition metal (TM)-based layered oxide electrocatalysts requiring lower η and demonstrating improved electrochemical performance toward OER have been reported recently [9,10].

Recently, larger interest has been shown in first-row TM-oxides (for instance, Cu, Co, Ni, and Fe) due to their enhanced electrochemical water splitting [11]. In particular, there has been significant interest in Cu-based oxidation electrocatalysts due to their natural abundance, low cost, rich redox chemistries, and non-toxic nature. Additionally, due to their low bandgap, they have been employed in several applications spanning from semiconductor, gas sensing, solar cells, and several biomedical applications [12–14]. However, their η values are still higher between 320–450 mV, which needs to be reduced significantly [15]. Another promising candidate is oxide of Mn (MnO_2), which displays enhanced electrochemical performances due to its unsaturated edges and possesses a wide variety of electronic structures, and its natural abundance is an added advantage [15]. This material has been widely used in other energy domains such as energy storage and electrochemical sensors for detecting metal ions [16–18]. Inheriting the benefit of CuO and MnO_2 by combining (CuO/ MnO_2), which is prepared hydrothermally, has been employed in catalytic applications for CO oxidations [19]. It is reported that CuO- MnO_2 interfaces serve as the active sites for CO oxidations and the chemisorbed CO on CuO reacts with the oxygen species in MnO_2 . This combination has also been reported to enhance electrochemical performances during the oxidation of quinolone at supercritical conditions and the proposed model dictates that the catalytic reaction strongly follows the temperature dependency [20–22].

Interfacial systems of similar structural and chemical complexity and their structural, chemical, and adsorption properties, including in relation to real-world applications, have been studied by using high-level DFT and ab initio molecular dynamics calculations [23]. Molecular modeling is regularly used for guiding and controlling the synthesis of various materials [24]. The nanosheet arrays of metal oxide/carbon (MO_x/C ; M = Fe, Ag, and Mn) fabricated and employed in the covered two-dimensional (2D) metal–organic frameworks (2D-MOFs) exhibiting significant electrocatalytic activity and durability [25]. Nb-doped TiO_2 rod-like particles were synthesized using molten salt as a reaction medium and applied as a catalyst support in ORR/OER bifunctional gas diffusion electrodes for use in metal–air batteries [26]. Ultrathin amorphous MnO_2 modified prawn-shell-derived porous carbon (U- MnO_2/PSNC) was designed and synthesized via a self-template-assisted pyrolysis coupling in situ redox reaction strategy to create robust oxygen electrocatalysts [27]. Fe_2O_3 decorated on carbon nanotubes as a promising architecture was utilized in OER reactions [28]. Pt alloy integrated in a cobalt–nitrogen–nanocarbon matrix 11.7 times higher

than that of a commercial Pt catalyst retained a stability of 98.7% after 30,000 potential cycles [29]. A carbon/rGO composite, as an efficient palladium electrocatalyst for formic acid oxidation reaction, was reported [30]. Developments in electrocatalyst corrosion chemistry, including corrosion mechanisms, mitigation strategies, and corrosion syntheses/reconstructions based on typical materials and important electrocatalytic reactions, have been extensively studied [31]. These interesting reports encouraged us to produce a CuO/MnO₂ system for electrocatalytic studies.

In the present study, we proposed a microwave-assisted synthetic protocol for the successful preparation of CuO and its interlaced architecture with MnO₂. The structural reliability and morphological properties of the composites were confirmed with the aid of XRD, FESEM, XPS, and EDS mapping. The surface property of CuO/MnO₂ was determined by BET analysis. As a proof-of-concept demonstration, we explored the virgin CuO and its composite CuO/MnO₂ for application in the oxygen evolution reaction. The CuO/MnO₂ exhibited an OER of 294 mV, which was evaluated with virgin CuO electrocatalyst (316 mV) at 10 mA cm⁻² and remained stable for 15 h. The synthetic procedure and the OER property of the prepared materials demonstrate its potential applications in electrocatalysis for the design of new hybrid materials.

2. Experimental Section

2.1. Materials and Reagents

The following materials of the highest purity were acquired from Sigma-Aldrich chemical (Korea) and applied without any further cleansing: CuSO₄·5H₂O, KMnO₄, Mn(CH₃COO)₂·4H₂O, and NaOH. Double-deionized water (DDW) was used for the preparation.

2.2. Syntheses of CuO

The protocol reported in [22] was utilized for preparing the CuO. Here, 20 mL of 0.2 M CuSO₄·5H₂O (20 mL) and 0.8 M NaOH (20 mL) solution were combined in a crucible and subjected to microwave irradiation for 10 min at 300 W. After completion of the reaction, the crude product was filtered, sequentially cleansed with deionized water to remove the water-soluble impurities, and ultimately dried at 80 °C. The obtained CuO was then utilized for electrocatalytic studies.

2.3. Syntheses of CuO/MnO₂

First, 0.2 M Mn(CH₃COO)₂·4H₂O (20 mL), 0.2 M KMnO₄ (20 mL), and 100 mg of CuO were placed in a crucible. The reaction mass was subjected to microwave irradiation for 15 min at 300 W. The solid product was then filtered, washed, and dried at 80 °C. Calcination of the resultant product for 6 h at 400 °C at a heating level of 5 °C/min resulted in pure CuO/MnO₂, which was then utilized for electrocatalytic studies.

3. Results and Discussion

Pristine CuO and its composite CuO/MnO₂ were prepared using a microwave-assisted synthetic protocol. The precursors CuSO₄·5H₂O, Mn(Ac)₂·4H₂O, and KMnO₄ were used for the formation of CuO/MnO₂ as illustrated in Figure 1. The suggested imitation route was ecologically friendly, as CuO is interlaced with MnO₂. Growth mechanism for the formation of CuO/MnO₂ structure, can be divided into three stages. Firstly, the MnO₄⁻ nuclei are produced and adsorbed on surfaces of CuO, forming MnO₂ nuclei. With the increase of reaction time, the MnO₂ nuclei are aggregated and transformed to nanosheets and nanorods. The MnO₂ nanorods are compact and totally cover surfaces of CuO, resulting in the formation of the hierarchical CuO/MnO₂ nanocomposites. Such a process is supported by the morphological evolution at different growth stages via tuning the reaction time. It is worth noting that the interconnected MnO₂ nanosheets and CuO nanostructure give rise to a highly porous morphology, which can offer very high surface area and many active sites for electrochemical transportation. X-ray diffraction (XRD) was used to study the

structural advancement and phase purity of the CuO and its composite CuO/MnO₂. As illustrated in Figure 2a, the phase analysis was conducted using XRD at Bragg's diffraction angle range was adjusted between 5°–65° during the measurement, and the scan rate was set to 2°/minute. The signals for planes (110), (002), (111), (202), (020), and (202) were, respectively observed at 32.4°, 35.6°, 38.7°, 48.9°, 53.3°, and 58.1° for the monoclinic CuO structure (JCPDS card no. 89-2529). However, after incorporating MnO₂, the supplementary diffraction heights detected at 2θ estimates of 12.7°, 15.6°, 18.0°, 37.6°, 40.6°, 42.0°, 49.9°, and 60.2° were, respectively credited to the (110), (001), (200), (121), (111) (301), (411), and (521) planes of the MnO₂ component (JCPDS card no. 72-1982 and 80-1098), which is crystalline [32,33]. The surface areas (BET) and pore size distribution (BJH) parameters were studied using N₂ adsorption–desorption isotherms as displayed in Figure 2, which demonstrated a characteristic IV isotherm that was ascribed to the mesoporous architecture of the aggregated CuO sphere, as displayed in Figure 2b. The CuO/MnO₂ revealed an enhanced volume and diameter of the pores, as shown in Figure 2c. The specific surface area for CuO/MnO₂ was found to be 54.50 m² g^{−1}, compared to 19.8 m² g^{−1} for pure CuO. The enhancement in surface area of the CuO/MnO₂ was a result of the combined porous MnO₂ nanorods.

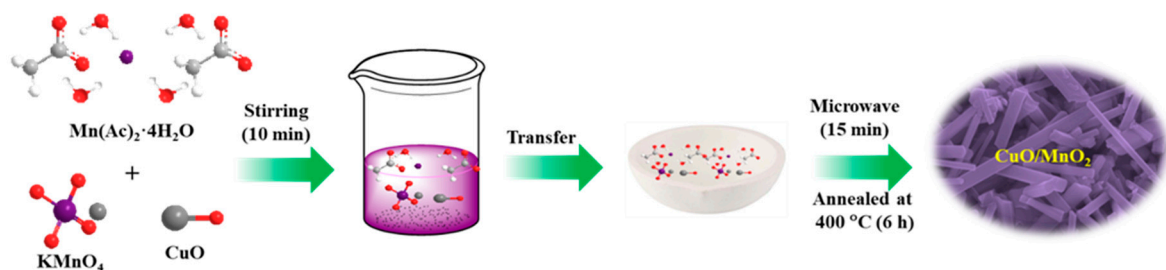


Figure 1. Schematics for synthesis of nanocomposite CuO/MnO₂.

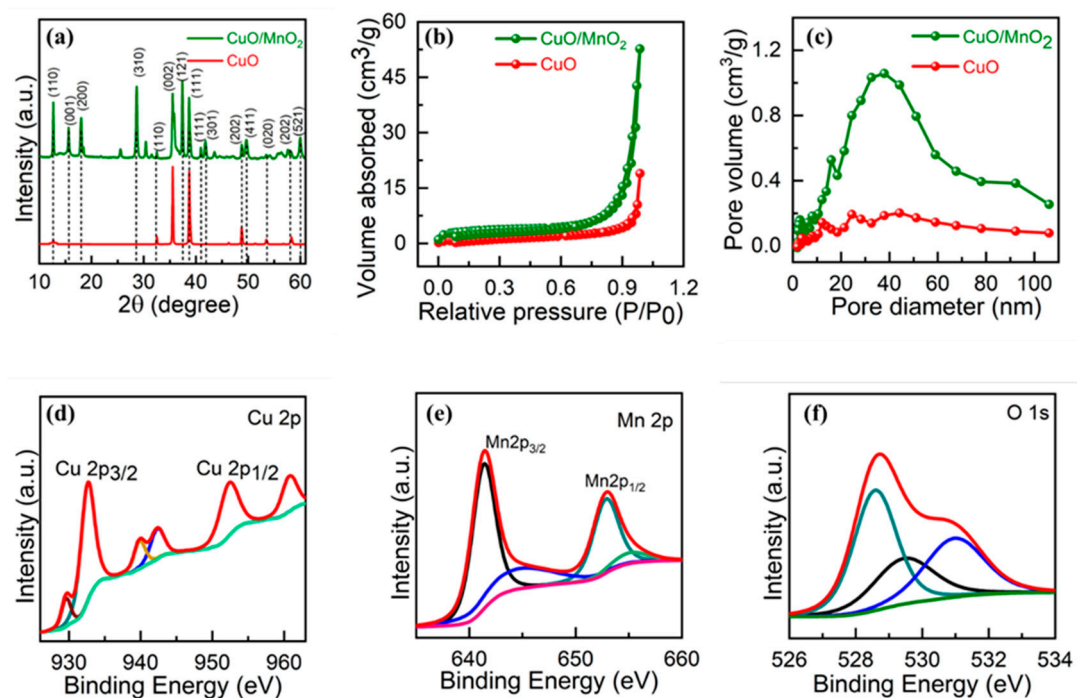


Figure 2. (a) XRD (b,c), BET data, and (d–f) XPS analysis of CuO/MnO₂ (a) Cu 2p, (b) O 1s, and (c) C 1s.

The valency and chemical binding on the surface of the combined material were studied using X-ray photoelectron spectroscopy (XPS) analyses. The XPS spectra of CuO/MnO₂

unveiled the manifestation of three elements (copper at 932.6 eV, manganese at 641.6 eV, and oxygen at 532.9 eV) on the exterior of the fused material. The binding powers of 932.6 and 952.4 eV referenced Cu 2p_{3/2} and Cu 2p_{1/2}, and a spin–orbit separation of 19.8 eV was exhibited for Cu 2p, as displayed in Figure 2d. Furthermore, two peaks were detected at 942.7 and 960.9 eV, which further confirmed that the sample contained CuO. The Mn 2p demonstrated peaks at 652.9 and 641.6 eV with a partition of 11.3 eV, as shown in Figure 2e, which is in agreement with the literature [34–36]. The CuO/MnO₂ presented a divided energy of 5.8 eV due to Mn–O in the existence of Cu²⁺. The O 1s exhibited three peaks (Figure 2f) at 532.4, 531.3, and 530.4 eV. The peaks of 532.4 and 531.3 were assigned to oxygen and moisture absorption on the composite surface. However, the peak at 530.4 eV agreed with the O²⁻ bonds with copper and manganese. Subsequently, the XPS results authorized the establishment of CuO/MnO₂ composite, and it was endorsed by XRD results. The survey spectra for CuO/MnO₂ are displayed in Figure S1.

The microstructure analysis of the CuO and CuO/MnO₂ was determined by scanning electron microscopy (SEM) and transmission electron microscopy (TEM), and the findings were reviewed in Figures 3 and 4. As illustrated in Figure 3a,b, the SEM images of CuO revealed the formation of amalgamated nanostructures. The energy-dispersive spectrometry (EDS) mapping directed the presence of O and Cu, as shown in Figure 3c,d.

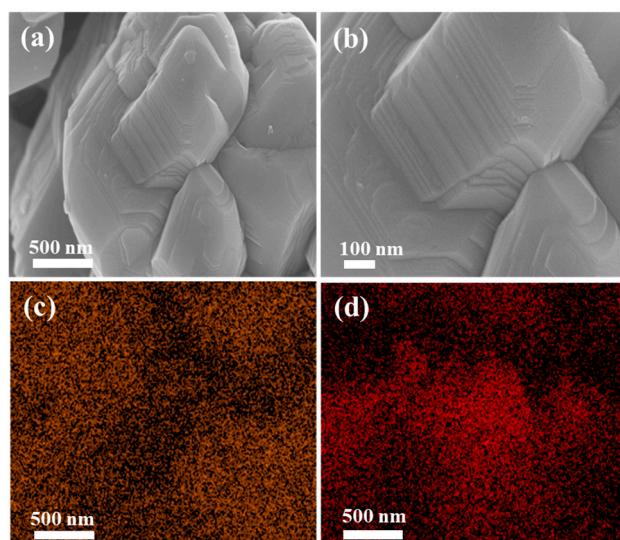


Figure 3. (a,b) SEM images; (c,d) EDX for CuO.

As shown in Figure 4a,b, CuO/MnO₂ was comprised of regular roads with negligible sheets at a 500 nanometer scale with accumulation. Moreover, at a greater enlargement, as shown in Figure 4b, the CuO/MnO₂ structures demonstrated a plane surface with clearly visible nanorods. Furthermore, the images of CuO@MnO₂ also confirm that MnO₂ was clearly interlaced with CuO. The elemental arrangement of the CuO/MnO₂ nanorod is exemplified in Figure 4c–f by energy-dispersive spectrometry (EDS) mapping, which indicated the presence of O, Cu, and Mn validating the effective construction of the composite.

The LSV behavior of the CuO and CuO/MnO₂ electrodes for OER was determined at a scan rate of 5 mV/s. Figure 5a displays the LSV curves of the CuO and CuO/MnO₂ electrodes. The overpotentials of the CuO and CuO/MnO₂ electrodes were 316 and 294 mV at a current density of 10 mA/cm², respectively (Figure S1). Moreover, the CuO/MnO₂ electrode exhibited a lower overpotential than that of the CuO electrode because of the enhanced intrinsic reaction kinetics and high catalytically active sites of the composite system of CuO/MnO₂. Furthermore, the overpotential of the prepared catalysts was closely related to the Tafel slope values. Figure 5b displays the Tafel curves of the prepared CuO

and CuO/MnO₂ electrodes. The Tafel values of the CuO and CuO/MnO₂ electrodes were determined from the following equation:

$$\eta = b \log (J) + a \quad (1)$$

where b , a , and η are the Tafel slope, arbitrary fitting parameter, and overpotential, respectively. The Tafel values of the CuO and CuO/MnO₂ electrodes were determined as 80 and 77 mV/dec, respectively. Compared to the CuO electrode, the CuO/MnO₂ electrode exhibited a low overpotential and a small Tafel value, due to its large number of catalytic active sites and the improved intrinsic reaction kinetics. The noted excellent electrocatalytic behavior had an impact on the electrochemical charge transfer kinetics, which can be seen through electrochemical impedance spectroscopy (EIS) measurement. Figure 5c presents the Nyquist plots of the CuO and CuO/MnO₂ electrodes, which were performed in a frequency range of 1 Hz to 10 kHz. The obtained semicircle at intermediate frequency range (1 Hz to 10 KHz) was attributed to the interfacial resistance within the grain itself. It affirmed that CuO/MnO₂ was exhibiting a low series resistance (R_s) of 1.85 Ohms and low charge transport resistance (R_{ct}) of 14.38 Ohms than the pure CuO-based electrode ($R_s = 1.92$ Ohm; $R_{ct} = 21.77$ Ohm). The EIS data are summarized in Table S1, revealing that the electron transport in the material interior, particularly at the CuO and MnO₂ interface, was increased compared to utilizing pure CuO, causing positively advanced electrocatalytically active sites that helped to improve the electrochemical reaction kinetics and yield better catalytic OER activity. Long-term potential stability is a crucial factor in catalysts for industrial purposes. Figure 5d presents the stability curve of the CuO/MnO₂ electrode at 10 mA/cm². The CuO/MnO₂ electrode clearly exhibited a stable static voltage curve at 15 h, indicating the excellent stable nature of the prepared materials. The Over potential, Tafel slope of CuO and CuO/MnO₂ is shown in Figure S2. Furthermore, the SEM images and XRD after OER confirms that the structure is retained (Figure S3). The embroidering layer of CuO/MnO₂ proposes conduction channels which speed up electron transport and fundamentally enrich the electrochemical properties [37–43]. A comparative table for the electrochemical OER performances of copper-based materials is shown in Table S2. The LSV polarization curve for IrO₂ catalyst is shown in Figure S4.

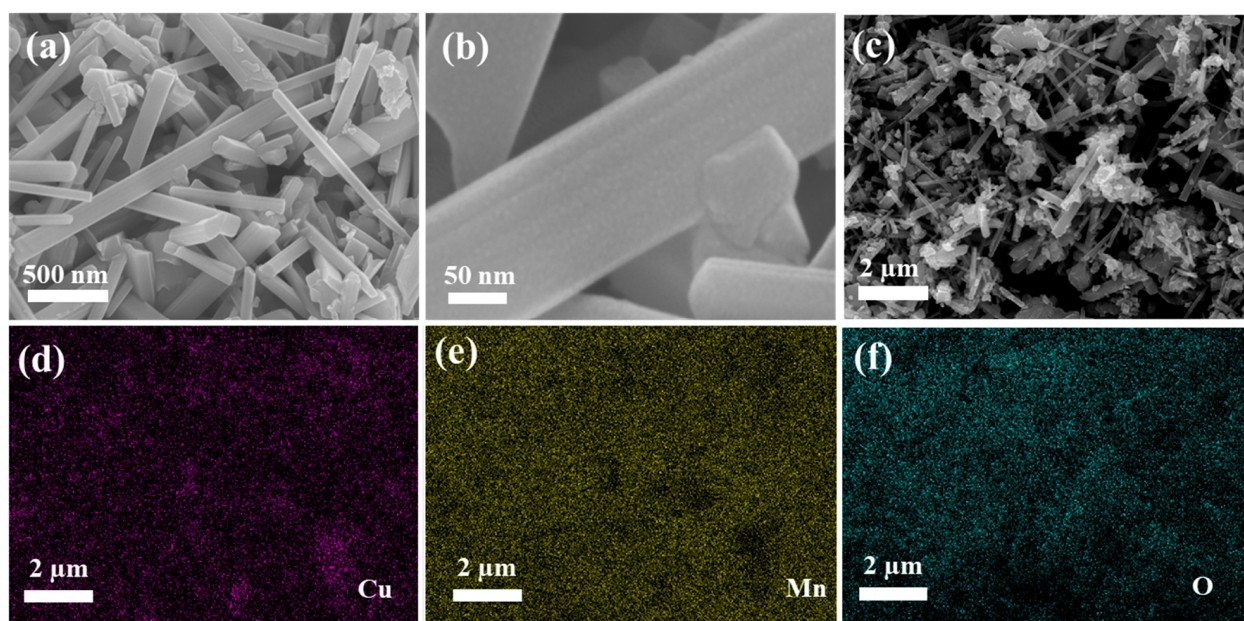


Figure 4. (a,b) SEM images; (c–f) EDX of CuO/MnO₂.

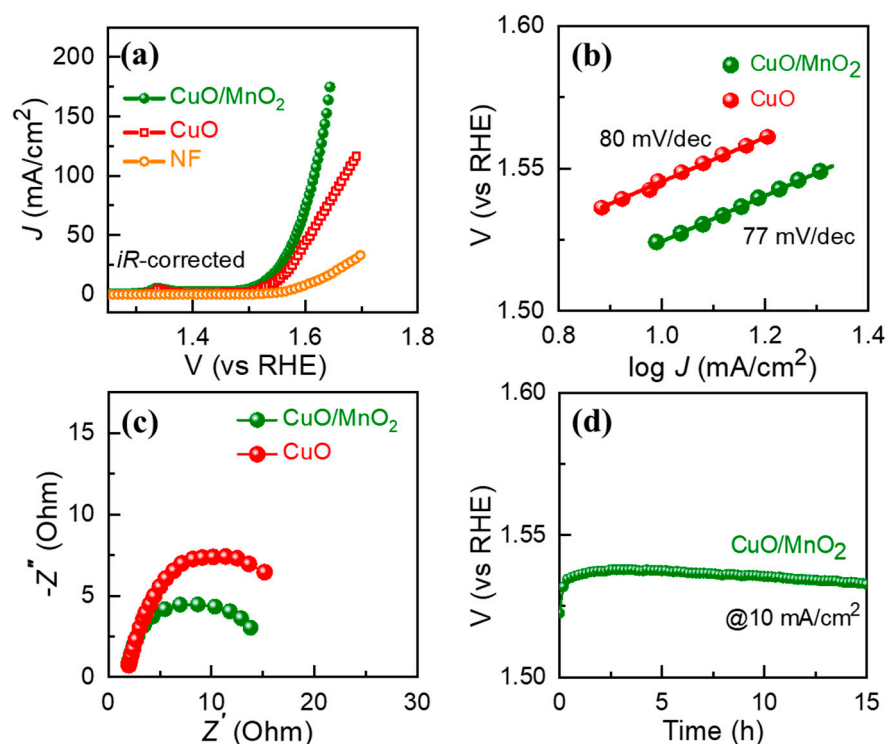


Figure 5. (a) iR-corrected LSV polarization curves, (b) Tafel plots, (c) Nyquist plots, and (d) long-term stability of the CuO/MnO₂ catalyst.

4. Summary and Conclusions

In summary, CuO and CuO/MnO₂ nano catalysts were synthesized using a green microwave-assisted protocol for utilization in OER. The prepared nano catalyst demonstrated the interlacing of CuO with MnO₂, required a minimal η of 294 mV to achieve a benchmark current density ($j = 10 \text{ mA cm}^{-2}$), and a superior stability of more than 15 h. These enhanced electrochemical performances are attributed to the large volume and expanded diameter of the pores, which offer ample surface area for catalytic reactions to boost OER. Furthermore, the rate kinetics of the OER were favored in composites due to a low Tafel slope (77 mV/dec) compared to CuO (80 mV/dec). The improved OER and long duration stability, along with the easy and scalable fabrication process of the CuO/MnO₂, offer a promising approach for the potential use of the electrode as an inexpensive catalyst material for electrochemical water-splitting applications.

Supplementary Materials: The following supporting information can be downloaded at: <https://www.mdpi.com/article/10.3390/nano13162329/s1>, Figure S1: XPS survey plot for CuO/MnO₂; Figure S2: (a) Over potential, (b) Tafel slope of CuO and CuO/MnO₂; Figure S3: (a) XRD after OER for CuO/MnO₂, (b) SEM image After OER; Table S1: Electrochemical impedance spectroscopy data for CuO and CuO/MnO₂; Table S2: Comparative table for electrochemical OER performances; Figure S4: The LSV polarization curve for IrO₂ catalyst. References [44–51] are cited in the supplementary materials.

Author Contributions: C.B.: Conceptualization, Investigation, Visualization, and Writing—original draft; A.M., Electrochemical Analysis; S.S., A.N.S., and R.S.; Investigation; A.E.-M., Electrochemical Analysis; R.R.P., Formal Analysis; H.-S.K., Conceptualization and Writing—review and editing. All authors have read and agreed to the published version of the manuscript.

Funding: This work was partly supported by the Mid-career Researcher Program through the National Research Foundation of Korea (NRF) funded by the Ministry of Science and ICT (No. 2019R1A2C2086747) and the research program of Dongguk University in 2022 (No. S-2022-G0001-00016). This work was also funded by the Researchers Supporting Project Number (RSPD2023R667), King Saud University, Riyadh, Saudi Arabia.

Data Availability Statement: All the experimental data presented within this article along with the supplementary information will be made available from the authors upon reasonable request.

Acknowledgments: We acknowledge the support of Mid-career Researcher Program through the National Research Foundation of Korea (NRF) funded by the Ministry of Science and ICT (No. 2019R1A2C2086747) and the research program of Dongguk University in 2022 (No. S-2022-G0001-00016). This work was also funded by the Researchers Supporting Project Number (RSPD2023R667), King Saud University, Riyadh, Saudi Arabia.

Conflicts of Interest: The authors declare no conflict of interest.

References

1. Singh, A.N.; Sandeep, K.; Janu, K.; Atanu, J.; Jin-Young, K.; Kwang, S.K. Interface Engineering Driven Stabilization of Halide Perovskites against Moisture, Heat, and Light for Optoelectronic Applications. *Adv. Energy Mater.* **2020**, *10*, 2000768. [[CrossRef](#)]
2. Tiwari, J.N.; Singh, A.N.; Sultan, S.; Kim, K.S. Recent Advancement of p- and d-Block Elements, Single Atoms, and Graphene-Based Photoelectrochemical Electrodes for Water Splitting. *Adv. Energy Mater.* **2020**, *10*, 2000280. [[CrossRef](#)]
3. Jeong, J.; Kim, M.; Seo, J.; Lu, H.; Ahlawat, P.; Mishra, A.; Yang, Y.; Hope, M.; Eickemeyer, F.; Kim, M.; et al. Pseudo-halide anion engineering for α -FAPbI₃ perovskite solar cells. *Nature* **2021**, *592*, 381–385. [[CrossRef](#)]
4. Sultan, S.; Jitendra, N.T.; Singh, A.N.; Shynggys, Z.; Miran, H.; Chang, W.M.; Pandiarajan, T.; Kwang, S.K. Single Atoms and Clusters Based Nanomaterials for Hydrogen Evolution, Oxygen Evolution Reactions, and Full Water Splitting. *Adv. Energy Mater.* **2019**, 1900624. [[CrossRef](#)]
5. McCrory, C.C.L.; Jung, S.; Peters, J.C.; Jaramillo, T.F. Benchmarking Heterogeneous Electrocatalysts for the Oxygen Evolution Reaction. *J. Am. Chem. Soc.* **2013**, *135*, 16977–16987. [[CrossRef](#)]
6. Yinlong, Z.; Wei, Z.; Yubo, C.; Jie, Y.; Meilin, L.; Zongping, S. A High-Performance Electrocatalyst for Oxygen Evolution Reaction: LiCo_{0.8}Fe_{0.2}O₂. *Adv. Mater.* **2015**, *27*, 7150–7155.
7. Zhiyi, L.; Haotian, W.; Desheng, K.; Kai, Y.; Po-Chun, H.; Guangyuan, Z.; Hongbin, Y.; Zheng, L.; Xiaoming, S.; Yi, C. Electrochemical tuning of layered lithium transition metal oxides for improvement of oxygen evolution reaction. *Nat. Commun.* **2014**, *5*, 4345.
8. Kaiyue, Z.; Tao, W.; Yue, Z.; Xuning, L.; Mingrun, L.; Ruifeng, L.; Wang, J.; Xuefeng, Z.; Weishen, Y. Layered Fe-Substituted LiNiO₂ Electrocatalysts for High-Efficiency Oxygen Evolution Reaction. *ACS Energy Lett.* **2017**, *2*, 1654–1660. [[CrossRef](#)]
9. Yinlong, Z.; Wei, Z.; Zhi-Gang, C.; Yubo, C.; Chao, S.; Moses, O.T.; Zongping, S. SrNb_{0.1}Co_{0.7}Fe_{0.2}O_{3- δ} perovskite as a next-generation electrocatalyst for oxygen evolution in alkaline solution. *Angew. Chem.* **2015**, *127*, 3969–3973.
10. Singh, A.N.; Kim, M.H.; Meena, A.; Wi, T.U.; Lee, H.W.; Kim, K.S. Na/Al Codoped Layered Cathode with Defects as Bifunctional Electrocatalyst for High-Performance Li-Ion Battery and Oxygen Evolution Reaction. *Small* **2021**, *17*, 2005605. [[CrossRef](#)]
11. Jamesh, M. Recent progress on earth abundant hydrogen evolution reaction and oxygen evolution reaction bifunctional electrocatalyst for overall water splitting in alkaline media. *J. Power Sources* **2016**, *333*, 213–236. [[CrossRef](#)]
12. Verma, N.; Kumar, N. Synthesis and Biomedical Applications of Copper Oxide Nanoparticles: An Expanding Horizon. *ACS Biomater. Sci. Eng.* **2019**, *5*, 1170–1188. [[CrossRef](#)] [[PubMed](#)]
13. Akhavan, O.; Ghaderi, E. Copper oxide nanoflakes as highly sensitive and fast response self-sterilizing biosensors. *J. Mater. Chem.* **2011**, *21*, 12935–12940. [[CrossRef](#)]
14. Pendashteh, A.; Mousavi, M.F.; Rahmanifar, M.S. Fabrication of anchored copper oxide nanoparticles on Graphene Oxide nanosheets via electrostatic coprecipitation and its application as supercapacitor. *Electrochim. Acta* **2013**, *88*, 347–357. [[CrossRef](#)]
15. Huang, M.; Li, F.; Dong, F.; Zhang, Y.X.; Zhang, L.L. MnO₂-based nanostructures for high-performance supercapacitors. *J. Mater. Chem. A* **2015**, *3*, 21380–21423. [[CrossRef](#)]
16. Husnain, S.M.; Asim, U.; Yaqub, A.; Shahzad, F.; Abbas, N. Recent trends of MnO₂-derived adsorbents for water treatment: A review. *New J. Chem.* **2020**, *44*, 6096–6120. [[CrossRef](#)]
17. Joya, K.; De Groot, J. Controlled Surface-Assembly of Nanoscale Leaf-Type Cu-Oxide Electrocatalyst for High Activity Water Oxidation. *ACS Catal.* **2016**, *6*, 1768–1771. [[CrossRef](#)]
18. Sohal, N.; Maity, B.; Shetti, N.P.; Basu, S. Biosensors Based on MnO₂ Nanostructures: A Review. *ACS Appl. Nano Mater.* **2021**, *4*, 2285–2302. [[CrossRef](#)]
19. Qian, K.; Qian, Z.; Hua, Q.; Jiang, Z.; Huang, W. Structure–activity relationship of CuO/MnO₂ catalysts in CO oxidation. *Appl. Surf. Sci.* **2013**, *273*, 357–363. [[CrossRef](#)]
20. Angeles-Hernández, M.J.; Leeke, G.A.; Santos, R.C. Catalytic supercritical water oxidation for the destruction of quinoline over MnO₂/CuO mixed catalyst. *Ind. Eng. Chem. Res.* **2009**, *48*, 1208–1214. [[CrossRef](#)]
21. Martin, A.; Armbruster, U.; Schneider, M.; Radnik, J.; Pohl, M.M. Structural Transformation of an Alumina-supported MnO₂-CuO oxidation catalyst by hydrothermal impact of sub- and supercritical water. *J. Mater. Chem.* **2002**, *12*, 639–645. [[CrossRef](#)]
22. Pengjiao, Z.; Li, W. Microwave-assisted synthesis of CuO/MnO₂ nanocomposites for supercapacitor application. *Micro Nano Lett.* **2020**, *15*, 938–942.
23. Davide, S.; Ricardo, F.; Gueorgui, G.; Anelia, K. Discovering atomistic pathways for supply of metal atoms from methyl-based precursors to graphene surface. *Phys. Chem. Chem. Phys.* **2023**, *25*, 5887.

24. Renato Batista, S.; Roberto, R.; Gueorgui, G.; Anelia, K. Exploring 2D structures of indium oxide of different stoichiometry. *Cryst. Eng. Comm.* **2021**, *23*, 6661–6667.
25. Owidah, Z.; Aman, S.; Abdullah, M.; Manzoor, S.; Fallatah, A.; Ibrahim, M.; Seaf Elnasr, T.; Mohd, Z. Ansari. Metal oxide/carbon nanosheet arrays derivative of stacked metal organic frameworks for triggering oxygen evolution reaction. *Ceram. Int.* **2023**, *49*, 5936–5943. [[CrossRef](#)]
26. Yuasa, M. Molten salt synthesis of Nb-doped TiO₂ rod-like particles for use in bifunctional oxygen reduction/evolution electrodes. *Ceram. Int.* **2022**, *48*, 14726–14735. [[CrossRef](#)]
27. Xiao, X.; Zhang, W.; Zhao, H.; Li, L.; Deng, P.; Wu, Y.; Luo, S.; Chen, B. Ultrathin amorphous MnO₂ modified prawn shells-derived porous carbon towards robust oxygen electrocatalyst for rechargeable Zn-air battery. *Ceram. Int.* **2022**, *48*, 6506–6511. [[CrossRef](#)]
28. Palem, R.; Meena, A.; Soni, R.; Meena, J.; Lee, S.; Patil, S.; Ansar, S.; Kim, H.; Im, H.; Bathula, C. Fabrication of Fe₂O₃ nanostructure on CNT for oxygen evolution reaction. *Ceram. Int.* **2022**, *48*, 29081–29086. [[CrossRef](#)]
29. Huang, L.; Wei, M.; Qi, R.; Dong, C.; Dang, D.; Yang, C.; Xia, C.; Chen, C.; Zaman, S.; Li, F.; et al. An integrated platinum-nanocarbon electrocatalyst for efficient oxygen reduction. *Nat. Commun.* **2022**, *13*, 6703. [[CrossRef](#)]
30. Ali, H.; Zaman, S.; Majeed, I.; Kanodarwala, F.; Nadeem, M.; Stride, J.; Nadeem, M. Porous Carbon/rGO Composite: An Ideal Support Material of Highly Efficient Palladium Electrocatalysts for the Formic Acid Oxidation Reaction. *Chem. Electro. Chem.* **2017**, *4*, 3126–3133. [[CrossRef](#)]
31. Li, F.; Huang, L.; Zaman, S.; Guo, W.; Liu, H.; Guo, X.; Xia, B. Corrosion Chemistry of Electrocatalysts. *Adv. Mater.* **2022**, *34*, 2200840. [[CrossRef](#)] [[PubMed](#)]
32. Wen, Z.Q.; Lia, M.; Li, F.; Zhu, S.J.; Liu, X.Y.; Zhang, Y.X. Morphology-controlled MnO₂-Graphene Oxides-diatomaceous earth 3-dimensional (3D) composites for high-performance supercapacitors. *Dalton Trans.* **2016**, *45*, 936–942. [[CrossRef](#)] [[PubMed](#)]
33. Zahan, M.; Podder, J. Structural, optical and electrical properties of Cu:MnO₂ nanostructured thin films for glucose sensitivity measurements. *SN Appl. Sci.* **2020**, *2*, 385. [[CrossRef](#)]
34. Racik, K.; Manikandan, M.; Mahendiran, M.; Prabakaran, P.; Madhavan, J.; Raj, M. Fabrication of manganese oxide decorated copper oxide (MnO₂/CuO) nanocomposite electrodes for energy storage supercapacitor devices. *Phys. E Low. Dimens. Syst. Nanostruct.* **2020**, *119*, 114033. [[CrossRef](#)]
35. Xie, Y.; Yang, C.; Chen, P.; Yuan, D.; Guo, K. MnO₂-decorated hierarchical porous carbon composites for high performance asymmetric supercapacitors. *J. Power Sources* **2019**, *425*, 1–9. [[CrossRef](#)]
36. Ramesh, S.; Kim, H.; Haldorai, Y.; Han, Y.; Kim, J. Fabrication of nanostructured MnO₂/carbon nanotube composite from 3D precursor complex for high-performance supercapacitor. *Mater. Lett.* **2017**, *196*, 132–136. [[CrossRef](#)]
37. Bathula, C.; Rabani, I.; Ramesh, S.; Lee, S.; Palem, R.; Ahmed, A.; Kim, H.; Seo, Y.; Kim, H. Highly efficient solid-state synthesis of Co₃O₄ on multiwalled carbon nanotubes for supercapacitors. *J. Alloys Compd.* **2021**, *887*, 161307. [[CrossRef](#)]
38. Rabani, I.; Zafar, R.; Subalakshmi, K.; Kim, H.-S.; Bathula, C.; Seo, Y.-S. A facile mechanochemical preparation of Co₃O₄@g-C₃N₄ for application in supercapacitors and degradation of pollutants in water. *J. Hazard. Mater.* **2020**, *407*, 124360. [[CrossRef](#)]
39. Rabani, I.; Yoo, J.; Bathula, C.; Hussain, S.; Seo, Y.-S. Role of uniformly distributed ZnO nanoparticles on cellulose nanofiber for flexible solid state symmetric supercapacitors. *J. Mater. Chem. A* **2021**, *9*, 11580–11594. [[CrossRef](#)]
40. Bathula, C.; Rabani, I.; Kadam, A.; Opoku, H.; Patil, S.A.; Shreshta, N.K.; Hwang, J.; Seo, Y.-S.; Kim, H.-S. Sonochemically exfoliated polymer-carbon nanotube interface for high performance supercapacitors. *J. Colloid. Interface Sci.* **2022**, *606*, 1792–1799. [[CrossRef](#)]
41. Palem, R.R.; Ramesh, S.; Rabani, I.; Shimoga, G.; Bathula, C.; Kim, H.S.; Seo, Y.S.; Kim, H.S.; Lee, S.H. Microstructurally assembled transition metal oxides with cellulose nanocrystals for high-performance supercapacitors. *J. Energy Storage* **2022**, *50*, 104712. [[CrossRef](#)]
42. Palem, R.R.; Ramesh, S.; Bathula, C.; Kakani, V.; Saratale, G.; Yadav, H.; Kim, J.; Kim, H.S.; Lee, S.H. Enhanced supercapacitive behavior by CuO@MnO₂/carboxymethyl cellulose composites. *Ceram. Int.* **2021**, *47*, 26738–26747. [[CrossRef](#)]
43. Ramesh, S.; Yadav, H.; Shinde, S.; Bathula, C.; Lee, Y.; Cheedarala, R.; Kim, H.; Kim, H.; Kim, J. Fabrication of nanostructured SnO₂@Co₃O₄/nitrogen doped graphene oxide composite for symmetric and asymmetric storage devices. *J. Mater. Res. Technol.* **2020**, *9*, 4183–4193. [[CrossRef](#)]
44. Liu, X.; Cui, S.; Sun, Z.; Ren, Y.; Zhang, X.; Du, P. Self-Supported Copper Oxide Electrocatalyst for Water Oxidation at Low Overpotential and Confirmation of Its Robustness by Cu K-Edge X-ray Absorption Spectroscopy. *J. Phys. Chem. C* **2016**, *120*, 831. [[CrossRef](#)]
45. Chauhan, M.; Reddy, K.P.; Gopinath, C.S.; Deka, S. Copper Cobalt Sulfide Nanosheets Realizing a Promising Electrocatalytic Oxygen Evolution Reaction. *ACS Catal.* **2017**, *7*, 5871–5879. [[CrossRef](#)]
46. Yang, L.; Xie, L.; Ren, X.; Wang, Z.; Liu, Z.; Du, G.; Asiri, A.M.; Yao, Y.; Sun, X. Hierarchical CuCo₂S₄ nanoarrays for high-efficient and durable water oxidation electrocatalysis. *Chem. Commun.* **2018**, *54*, 78–81.
47. Kuang, M.; Han, P.; Wang, Q.; Li, J.; Zheng, G. CuCo Hybrid Oxides as Bifunctional Electrocatalyst for Efficient Water Splitting. *Adv. Funct. Mater.* **2016**, *26*, 8555–8561. [[CrossRef](#)]
48. Ahmed, A.; Hou, B.; Chavan, H.; Jo, Y.; Cho, S.; Kim, J.; Pawar, S.; Cha, S.; Inamdar, A.; Kim, H.; et al. Self-Assembled Nanostructured CuCo₂O₄ for Electrochemical Energy Storage and the Oxygen Evolution Reaction via Morphology Engineering. *Small* **2018**, *14*, 1800742. [[CrossRef](#)]

49. Yan, H.; Wang, X.; Linkov, V.; Ji, S.; Wang, R. Selectivity Evolution Reaction on Carbon Cloth-Supported δ -MnO₂ Nanosheets in Electrolysis of Real Seawater. *Molecules* **2023**, *28*, 854. [[CrossRef](#)]
50. Zheng, X.; Qin, M.; Ma, S.; Chen, Y.; Ning, H.; Yang, R.; Mao, S.; Wang, Y. Strong Oxide-Support Interaction over IrO₂/V₂O₅ for Efficient pH-Universal Water Splitting. *Adv. Sci.* **2022**, *9*, 2104636. [[CrossRef](#)]
51. Wang, Q.; Huang, X.; Zhao, Z.L.; Wang, M.; Xiang, B.; Li, J.; Feng, Z.; Xu, H.; Gu, M. Ultrahigh-Loading of Ir Single Atoms on NiO Matrix to Dramatically Enhance Oxygen Evolution Reaction. *J. Am. Chem. Soc.* **2020**, *142*, 7425–7433. [[CrossRef](#)] [[PubMed](#)]

Disclaimer/Publisher's Note: The statements, opinions and data contained in all publications are solely those of the individual author(s) and contributor(s) and not of MDPI and/or the editor(s). MDPI and/or the editor(s) disclaim responsibility for any injury to people or property resulting from any ideas, methods, instructions or products referred to in the content.